

On the faint end of the high redshift AGN luminosity function

Francesco Shankar & Smita Mathur

Astronomy Department, Ohio State University, 140 W. 18th Ave., Columbus, OH-43210, U.S.A.
shankar, smita@astronomy.ohio-state.edu

ABSTRACT

Using the results of recent optical surveys we conclude that the *non*-detection of quasars down to faint magnitudes implies a significant flattening of the high redshift ($z \sim 6$) optical active galactic nuclei (AGN) luminosity function for $M_{1450} > -26.7$. We find that all the data are consistent with a faint-end slope for the optical AGN luminosity function of $\beta = -2.2$ and $\beta = -2.8$, at the 90% and 99% confidence level respectively, flatter than the bright-end slope of $\beta' \sim -3.2$. We also show that X-ray deep surveys have probed even fainter magnitudes than the optical ones yielding more significant constraints on the shallow faint-end slope of the optical luminosity function. The inclusion of Type II AGN candidates, detected in the *Chandra* deep fields, hints towards an higher normalization for the total AGN luminosity function, if these sources lie at $5 \lesssim z \lesssim 6.5$. We then discuss simple theoretical models of AGN formation and evolution in the context of cold dark matter cosmology. The comparison with the total AGN luminosity function favors a redshift-dependent relation between black hole and dark matter halo masses of the type $M_{\bullet} \propto M_{\text{halo}}^{\alpha}$, with $1.3 \lesssim \alpha \lesssim 1.7$, compatible with independent studies from statistical analysis and rotation curve measurements. Finally we compute the quasar contribution to reionization to be $\lesssim 9\%$ at $z \sim 6$, up to $\sim 30\%$ when integrated within $5.5 \lesssim z \lesssim 6.5$, significantly smaller than that from galaxies.

Subject headings: galaxies: active - quasars:general

1. Introduction

A fundamental tool to study the evolution of Active Galactic Nuclei (AGNs) is their luminosity function (LF) and its evolution with redshift. This enables us to probe the accretion history of Super-massive Black Holes (SMBHs) which, in turn, set constraints on galaxy evolution, as SMBHs are believed to be ubiquitous and tightly linked with all stellar bulges and spheroids today (e.g. Ferrarese & Ford 2005 and references therein). Moreover constraining the AGN LF is essential to understand the AGN contribution to the total emissivity background in different bands, their environmental impact, their clustering properties and the role AGNs had, if any, in the cosmological re-ionization of Hydrogen and Helium.

X-ray observations carried out with *Chandra*, *ASCA*, *HEAO-1* are statistically complete in X-ray to a level of $\sim 90\%$ up to $z \sim 3 - 4$ (e.g. La

Franca *et al.* 2005). These observations have assessed that AGNs statistically follow a luminosity-dependent density evolution (e.g. Ueda *et al.* 2003), in which lower luminous AGNs peak at $z \lesssim 1$, while higher luminous ones, usually optically bright, peak at higher redshifts, $z \sim 2$ (e.g. Osmer 2004). However how far in time can we track AGN evolution? The picture is still not yet complete at higher redshifts, where X-ray measurements of the AGN LF are lacking.

On the optical side the SDSS team (Richard *et al.* 2006), and earlier works by Kennefick *et al.* (1995), COMBO-17 (Wolf *et al.* 2003) have probed the bright tail of the optical AGN LF up to $z \sim 4.7$ down to magnitudes of $M_{1450} \lesssim -23.3$ showing that a simple power-law can easily fit the data. The GOODS team (Cristiani *et al.* 2004; Fontanot *et al.* 2006a) has been able to set constraints on the shape of the optical LF down to

$M_{1450} \sim -21.5$ and up to $z \sim 5$, showing evidence for a flattening at the faint-end. Fan *et al.* (2004; F04 from here on) have instead probed the very luminous tail of the $z \sim 6$ optical LF up to $M_{1450} \lesssim -26.5$.

Here we use existing observations of optically selected AGN and *Chandra* deep fields to determine constraints on the redshift 6 shape of both the optical and X-ray LF. We will in particular show that X-ray observations allow us to probe the $z \sim 6$ LF to ~ 2 magnitudes fainter than the deepest optical observations. In section 2 we describe our method, present the constraints on the faint end LF in section 3, their implications in sections 4 and 5, and conclude in section 6. We use concordance cosmological parameters $\Omega_m = 0.27$, $\Omega_\Lambda = 0.73$, $\Omega_b = 0.022h^{-2}$, $H_0 = 71 \text{ km s}^{-1} \text{ Mpc}^{-1}$, $\sigma_8 = 0.84$, and $\Gamma = 0.2$ (Spergel *et al.* 2003).

2. Method

In the following we will always call AGNs the total population of Active Galactic Nuclei, while we will refer to Type I, optical AGNs as "QSOs" (or "quasars") and we'll simply call Type II AGNs those which have a column density above $\log N_H = 22 \text{ cm}^{-2}$ and are often very faint or even missed in optical surveys, but still detected in X-rays.

Several deep X-ray and optical surveys have now probed several portions of the AGN luminosity function at high redshifts, however often finding a scarce number of faint sources. In this paper we will show that the paucity of sources at these faint fluxes gives the most up-to-date stringent constraints on the knee and the faint-end slope of the QSO LF and give hints to the overall AGN distribution at $z \sim 6$. Similar studies, though with looser upper limits, have been carried out by Sharp *et al.* (2004), Willott *et al.* (2005), Wyithe (2004) and Dijkstra & Wyithe (2006).

To convert X-ray to optical rest-frame luminosities we will use the equation (see Richards *et al.* 2005)

$$\log L_{2 \text{ keV}} = \log L_{2500} + \alpha_{\text{ox}} \log \left(\frac{\nu_{2 \text{ keV}}}{\nu_{2500}} \right), \quad (1)$$

between monochromatic luminosities and a constant photon index $\Gamma = 1.8$ to compute the broad-

band X-ray luminosities. Many authors (e.g. Vignali *et al.* 2003) have found that the spectral index α_{ox} depends significantly on luminosity. In particular the latest results by Steffen *et al.* (2006), who have collected a large number of optically and X-ray selected AGNs at several redshifts, claim a significant correlation of the spectral index with luminosity and a marginal one (1.1σ) with redshift, i.e.

$$\alpha_{\text{ox}} = (-0.126 \pm 0.013) \log L_{2500} - (0.01 \pm 0.009)z + (2.311 \pm 0.372), \quad (2)$$

where L_{2500} is the monochromatic luminosity at 2500 \AA , in units of $\text{erg s}^{-1} \text{ Hz}^{-1}$.

In the following we will use results from several optical/NIR surveys carried out on different areas. To compare the luminosities probed by different observations, we will first need to convert the broadband z_{AB} , where most of the observations are carried out, to the apparent magnitude at wavelength $1450(1+z) \text{ \AA}$, i.e. $AB_{1450(1+z)}$, and finally convert the latter to the rest-frame luminosities M_{1450} .

We convert z_{AB} to $AB_{1450(1+z)}$ magnitude following the spectrum described in Cristiani & Vio (1990) and updated in Cristiani *et al.* (2004). To convert then to absolute magnitudes M_{1450} , we note that in the AB system $m_{\text{AB}} = -2.5 \log f_\nu - 48.6$, where the monochromatic flux f_ν is in units of $\text{erg cm}^{-2} \text{ s}^{-1} \text{ Hz}^{-1}$, and the absolute magnitude is $M_{\text{AB}} = -2.5 \log L_{\nu(1+z)} + 51.6$, where $L_{\nu(1+z)}$ is the luminosity at rest frame frequency $\nu(1+z)$, in units of $\text{erg s}^{-1} \text{ Hz}^{-1}$. Using $f_\nu = (1+z)L_{\nu(1+z)}/4\pi D_L^2(z)$ leads to (see also Stern *et al.* 2000b)

$$M_{1450} = AB_{1450(1+z)} + 2.5 \log(1+z) + 97.45 - 5 \log D_L(z) \quad (3)$$

and (Fan *et al.* 2001)

$$M_B = M_{1450} + 2.5\alpha \log(4400/1450) + 0.12 \quad (4)$$

where M_B is the absolute B magnitude calibrated for a $f_\nu \propto \nu^\alpha$ (where we set $\alpha = -0.5$) spectrum and the factor 0.12 comes from the zero point difference between the AB and Vega-based system (Fan *et al.* 2001).

To constrain the shape of the $z \sim 6$ AGN LF, following Willott *et al.* (2005), we first define a

double power-law model LF of the type

$$\Phi(M_{1450}, z) = \frac{dn(M_{1450}, z)}{dM} = \rho(z) \times \frac{\Phi_0}{10^{0.4(\beta+1)(M_{1450}-M_{1450}^*)} + 10^{0.4(\beta'+1)(M_{1450}-M_{1450}^*)}}, \quad (5)$$

where $\rho(z) = 10^{-0.48(z-z_0)}$, with $z_0 = 6.07$, is the average redshift of the F04 LF. With such a parametrization we assume that the high-redshift AGN LF evolves with a Pure Density Evolution (PDE) beyond redshift of 5 at the same rate as the LF in Fan *et al.* (2001). Following the observations by F04, Φ_0 has been calibrated to match the cumulative number density of $\sim 6.4 \times 10^{-10} \text{ Mpc}^3$ for sources with $M_{1450} < -26.7$ at $z = z_0$ (these are the limit and number density for $\Omega_m = 0.35$, $\Omega_\Lambda = 0.65$, $H_0 = 65$ and have been converted to our cosmology). The bright-end slope and the break magnitude have been fixed to $\beta' = -3$ and $M_{1450}^* = -24.67$ respectively, as this provides a very good match to the Cool *et al.* 2006 observations (see below). The faint-end slope β has been left variable and constrained by matching the observed number density of sources in each survey. At $z \sim 5$ the LF in equation (6) is in agreement with the cumulative number density determined by Fan *et al.* (2001).

Thus given a model LF we integrate it within the effective volume of the survey using the following equation (see e.g. Fan *et al.* 2001)

$$n_{\text{obs}} = \Delta\Omega \int_{z_{\text{min}}}^{z_{\text{max}}} dz \frac{dV}{dz d\Omega} \times \int_{L_{\text{min}}(z)}^{\infty} \Phi(L, z) dL p(L, z, \text{SED}), \quad (6)$$

and tune the faint-end slope β in equation (6) to match the observed number of sources n_{obs} in the survey. $L_{\text{min}}(z)$ refers to the redshift dependent absolute luminosity, corresponding to the minimum optical apparent magnitude (or the minimum flux) considered. We will in general assume a constant selection function $p(L, z, \text{SED})$ for each survey, as indicated by the authors or derived from their papers. In the following we will always use the form in equation (6) for $\Phi(L, z)$, unless in some specified cases, in which we will adopt the Fan *et al.* (2001) LF. The latter is a single power-law function valid in the range $4 < z < 5.5$, in which we let the slope β_0 to be variable, while we keep

the redshift evolution and normalization at M_{1450}^* as in Fan *et al.* (2001; both M_{1450}^* and normalization have been converted to our cosmology, which is required at each redshift bin during the evolution).

3. Results

3.1. The Type I AGN Luminosity Function

A significant improvement with respect to previous works has been to fix the knee of the LF in equation (6) to the value recently inferred by Cool *et al.* (2006). These authors discovered three objects down to $z_{\text{AB}}=21.93$, (i.e. $M_{1450} \sim -24.67$ at $z = 5.53$ using equation (4)) in the AGN and Galaxy Evolution Survey (AGES) spectroscopic observations of the NOAO Deep Wide-Field Survey (NDWFS). They covered 7.7 deg^2 of the NDWFS field with an average completeness level of 54% down to $I_{\text{AB}} = 22 \text{ mag}$. These authors claim their observations agree with the F04 LF with a slope of $\beta = -3.2$ and a redshift evolution as in Fan *et al.* (2001) and in equation (6). Using equation (7), we find ~ 3 sources with $z_{\text{AB}} \gtrsim 21.93$ at $z > 5$, in very good agreement with observations and with the authors. The integration was pursued up to $z = 7$, as beyond this limit the optical selection of quasars becomes impossible because the Ly α line redshifts out of the z_{AB} -band (see Cool *et al.* 2006).

Following a similar procedure we find significant evidence for a flattening of the QSO LF below $M_{1450} \sim -24.67$. Recently, Mahabal *et al.* (2005, M05 hereafter) in the field around the $z = 6.42$ quasar SDSS J1148+5251 discovered a quasar at redshift $z = 5.70$ with luminosity of $M_{1450} \sim -23.6$, i.e. $z_{\text{AB}} = 23.0$. This quasar is the faintest known optically selected quasar at $z > 5.5$, allowing determination of the faint end of the quasar LF to fainter luminosities.

The authors claim the source, identified in a $\sim 2.5 \text{ deg}^2$ survey, has a surface density consistent with the Wolf *et al.* (2003) LF extrapolated through a PDE within their effective volume, which follows the R -band drop-out criterion of Stern *et al.* (2000), i.e. $4.3 \lesssim z \lesssim 5.8$. We have checked that adopting the latter determination for the effective volume, we recover the results of the authors only if an average $\sim 28\%$ selection detec-

tion probability is used. However using the Wolf *et al.* (2003) LF, which is defined only for $z \lesssim 4.7$, needs an extrapolation to higher redshifts. Moreover the functional form in equation (6) has been calibrated on the data by Cool *et al.* (2006) at $z \gtrsim 5$. We therefore replace equation (6) with the Fan *et al.* (2001) QSO LF, more appropriate for the redshift bin probed by the *R*-band drop-out technique.

Keeping the same value for the selection function we find that the detection of one object in the effective volume probed by M05, is consistent with a number density at $M_{1450} \sim -23.6$ of $\log[dn/dM] \sim -6.70$ at the 99% confidence level (CL; with $\beta_0 = -2.8$), down to $\log[dn/dM] \sim -6.95$ at the 90% CL (with $\beta_0 = -2.54$; see Table 1; we plot the M05 data in Figure 1 shifted by -0.15 magnitudes for avoiding overcrowding with Willott *et al.*'s data). Their data, shown as solid triangles in Figure (1), are consistent with extrapolating equation (6) to fainter optical magnitudes using $\beta = -2.3$ and $\beta \sim -1.7$ at the 99% and 90% CL respectively (see Table 1). Note that these are conservative estimates. Extending the computation of the LF down to the limiting magnitude of the M05 survey ($z_{AB} = 24.5$, $M_{1450} \sim -22$) or using a higher completeness function would yield even lower limits on β .

Willott *et al.* (2005) undertook a multicolor quasar optical imaging with the Canada-France-Hawaii Telescope. They found a lack of quasars down to a limiting magnitude of $z_{AB} = 23.35$ (i.e. $M_{1450} \sim -23.63$ at $z = 6.1$; see Figure 1). The few detected quasar candidates had been subsequently rejected as being identified with low-mass stars in the near-infrared follow-up imaging. Using equations (6) and (7), we find that the Willott *et al.* (2005) results are consistent with a faint-end slope of $\beta = -2.97$ at 99% CL, down to $\beta = -2.4$ at the 90% CL. We use the selection function computed from simulated colors for high-redshift QSOs in the redshift range $5.5 \lesssim z \lesssim 6.7$ (see Figure 2 in Willott *et al.* 2005). This is the most conservative selection function from Willott *et al.* (2005), determined for very extreme red color cuts. Using a less conservative estimate (solid line in their Figure 2) our results drop to $\beta = -2.84$ at 99% CL, down to $\beta = -2.2$ at the 90% CL.

The above findings are shown in Figure 1. The gray area shows the data with its 1σ -error bars by

F04 for the $z \sim 6.1$ LF, while the solid dots show the extrapolation of the F04 LF to faint luminosities assuming a single slope of $\beta = -3.2$. The presence of a significant downturn in the QSO LF for magnitudes below $M_{1450} \sim -24.67$ is evident. In particular the M05 observations are significantly stringent in constraining the faint-end slope.

In Figure 1 we also show the interesting result by Stern *et al.* (2000). These authors have discovered a quasar at $z = 5.50$ from deep, multicolor, ground-based observations covering 74 arcmin² with $z_{AB} = 23.4$. To estimate their average selection function we redo the calculations in Stern *et al.* (2000) and integrate down to $M_B = 22.5$ (in their cosmology) the Boyle *et al.* (1991) $z = 2$ quasar LF, evolved as in Schmidt *et al.* (1995). The effective volume probed is again defined by the *R*-band drop-out as in M05 (Stern *et al.* 2000). We find that an average completeness of $p = 0.89$ recovers their quoted ~ 0.15 quasars in the field of view. As for M05, we then use the more up-to-date Fan *et al.* (2001) LF, more suitable for the redshift range probed by this survey, and equation (7). Even in this case we let the slope to be variable, $\beta_0 = -2.92$ in the specific case, while we keep the redshift evolution and normalization at M_{1450}^* as in Fan *et al.* (2001).

We integrate down to $AB_{1450(1+z)} = 24.1$ (see Table 1 in Stern *et al.* 2000), instead of using the measured $z_{AB} = 23.4$. This is because the authors find their source to have unusual spectral features for which they derive a special continuum model which is significantly different from the average spectral template used in this paper. The detection of one source in their field of view is consistent with a comoving density of $\log[dn/dM(-22.5, 5.5)] \sim -5.66 \text{ Mpc}^{-3} \text{ mag}^{-1}$, lower than the F04 extrapolation at the $\gtrsim 80\%$ CL (see Figure 1). The number density we find still shows evidence for a turnover in the QSO LF expressed in equation (6), with $\beta = -2.8$, though less significant than the above results, in agreement with the authors.

We now turn to the analysis of X-ray data. Barger *et al.* (2003; see also Cowie *et al.* 2003) have used deep multicolor optical data to search for $z > 5$ AGNs in the 2 Ms X-ray *Chandra* Deep Field-North exposures. They found 500 sources in their field of view out of which 423 have $z_{AB} < 25.2$. Color analysis was carried out on all

TABLE 1
FAINT-END SLOPES FOR THE QSO LF AT SEVERAL CONFIDENCE LEVELS

survey	$ \beta $	90%	95%	99%	Area	p
Mahabal et al.		1.7	1.9	2.3	2.5 sq. deg.	28 %
Willott et al.		2.27	2.57	2.95	3.32 sq. deg.	variable
Barger et al. (single source)		2.32	2.38	2.48	160 arcmin ²	50 %

NOTE.—All the values in the first three columns give the faint-end slopes β (equation (6)) needed to reproduce the observed number density in each survey; all confidence levels are computed through Poissonian statistics following Gehrels *et al.* (1986); the column before last indicates the effective area probed by each survey; the last column indicates the average selection function used for each survey.

the sources, while 249 sources have spectroscopically confirmed redshifts. Of these, only one object was found at $5 < z < 6$ and none at $z > 6$. They found a faint AGN at $z = 5.19$ with $z_{AB} = 23.9$, corresponding to an absolute magnitude of $M_{1450} \sim -22.8$, i.e. nearly a magnitude fainter than the M05 source, showing the power of X-ray observations. Barger *et al.* (2003) claim that none of the spectroscopically unidentified sources with $z_{AB} < 25.2$ is red enough to have $z > 5$. With the aid of the V/V_{\max} method the authors estimated the LF in the comoving volume $5 < z < 6.5$ to be consistent with the extrapolation of the Fan *et al.* (2001) LF with a slope of $\beta = -2.6$ in the luminosity bin $43 \leq \log L_{2-10 \text{ keV}} \leq 44$ (in erg s^{-1}).

Here we proceed with a similar calculation but using equation (7) and extrapolating the Fan *et al.* (2001) LF at redshifts beyond $z \sim 5$, in the same manner as for computing the number density in Stern *et al.* (2000). We find that the number of observed sources down to $z_{AB} = 25.2$ integrated between $5 \lesssim z \lesssim 6.5$, with $\beta = -2.1$ and a completeness of $p = 0.7$ (Cowie *et al.* 2002) is ~ 1 , in very good agreement with observations. We considered an area of 160 arcmin², corresponding to the solid angle where the hard X-ray flux limit has a signal-to-noise ratio of $S/N=3$ (see Figure 19 in Alexander *et al.* 2003).

The X-ray flux considered here is $f_{0.5-8 \text{ keV}} \approx 2.5 \times 10^{-16} \text{ erg cm}^{-2} \text{ s}^{-1}$ (Alexander *et al.* 2003; Barger *et al.* 2003). This flux limit is the minimum level of X-ray flux which corresponds to an

optical magnitude brighter than $z_{AB} = 26.9$ (the optical detection limit in Barger *et al.* (2003)) within the whole effective volume considered. This is required as all the 500 sources in the CDFN have optical colors. We find a number density of $\log [dn/dM(-21.4, 5.7)] \sim -5.66$ ($\text{Mpc}^{-3} \text{ mag}^{-1}$) corresponding to $\log L_{2-10 \text{ keV}} \sim 43.6$ (erg s^{-1}) (equation (3)), a factor of 2 – 3 higher, but broadly consistent, with the results by Barger *et al.* (2003; plotted in Figure 1 as an open circle with its 99% CL error bars).

Indeed deep X-ray observations effectively allow us to probe even fainter optical luminosities. Mathur *et al.* (2002; Brandt *et al.* 2002) detected three $z \sim 6$ quasars discovered by Fan *et al.* (2001b) with *Chandra* with exposure times of less than 10 ksec. The objects are detected in X-rays up to 55 keV in rest frame, demonstrating the incredible sensitivity of *Chandra* to detect faint sources. The faintest quasar in their sample, SDSS 1030+0524, at $z = 6.28$ was detected in about 8 ksec with an observed flux of $f_{0.5-8 \text{ keV}} = 4 \times 10^{-15} \text{ erg cm}^{-2} \text{ s}^{-1}$. The *Chandra* deep field observations have exposure time of 2 Msec, so could detect down to $2000/8 = 250$ times fainter sources with a flux limit of $f_{0.5-8 \text{ keV}} \approx 1.6 \times 10^{-17} \text{ erg cm}^{-2} \text{ s}^{-1}$. This however would be the sensitivity limit at the aim point, close to the aim point sensitivity reported by Alexander *et al.* (2003). Therefore we expect the *Chandra* observations to be sensitive in detecting sources down the minimum flux considered, i.e. we can extend the

computation using equation (7) down to the limit of $f_{0.5-8\text{ keV}} \approx 2.5 \times 10^{-16} \text{ erg cm}^{-2} \text{ s}^{-1}$ (i.e. down to $z_{\text{AB}} \sim 26$ at the average redshift of $z = 5.7$). In Figure 1 and Table 1 we report our findings. Using a completeness of about 50%, as computed by Cowie *et al.* (2002) for faint fluxes (notice that the use of an higher completeness level would strengthen our results), we find that the detection of a single source in the *Chandra* Deep Field in the range $5 < z < 6.5$, is consistent with a faint slope of $\beta = -2.48$ at the 99% CL, down to $\beta = -2.32$ at the 90% CL (shown as solid squares).

Barger *et al.* (2003) claim that none of the unidentified sources is red enough to be at $z > 6$. They however also point out that up to nine out of the optically faint spectroscopically unidentified sources with $z_{\text{AB}} > 25.2$, could still possibly lie in the range $5 < z < 6.5$. Therefore assuming these sources to rely in the same luminosity bin as the single $z = 5.19$ source, they find an upper limit to their comoving LF about an order of magnitude higher than their previous estimate. Following the same approach undertaken for the case of a single source, we apply equation (7) using Fan *et al.* (2001) down to $f_{0.5-8\text{ keV}} \approx 2.5 \times 10^{-16} \text{ erg cm}^{-2} \text{ s}^{-1}$ and using a completeness of $p = 0.5$, proper for faint fluxes (Cowie *et al.* 2002). We consider all the nine sources not to be heavily obscured, i.e. they are Type I AGN. We find that the comoving number density of the LF to be $\log[dn/dM(-20.6, 5.7)] \sim -4.52 \text{ (Mpc}^{-3} \text{ mag}^{-1})$, using a slope $\beta = -2.57$ (shown as an open square with its 99% CL in Figure 1). Our estimate is higher but still consistent with the one by Barger *et al.* (2003). To notice also that our estimate is also quite conservative, lower limits would be inferred extending the computation to lower magnitudes, close to the survey limit ($z_{\text{AB}} = 26.9$).

The $1\text{-}\sigma$ uncertainties in equation (1) produce uncertainties of ~ 0.15 magn in the final computation of the optical M_{1450} magnitude, as shown in Figure 1. We also notice that our conclusions are quite insensitive to the actual fit used for the optical-to-X-ray flux ratios. For example, similar results are also obtained using the relation between luminosity in the rest-frame R band, L_R , and the hard X-ray luminosity $L_{2-10\text{ keV}}$ calibrated by La Franca *et al.* (2005; see their equation (4)) for Type I AGNs. The Vignali *et al.*

(2003) fit instead of equation (1) would yield even fainter optical magnitudes for the same X-ray flux and number density, thus strengthening our results for a presence of a flattening at the faint-end of the QSO LF.

We conclude this section noting that all the data are consistent with a break in the QSO LF at $M_{1450} \gtrsim -24.67$. The faint-end slope of the *optical* Type I AGN LF, is consistent with being on average $\beta \sim -2.2$, at the 90% CL and $\beta \sim -2.8$, at the 99% CL (see Figure 1). Our overall findings are consistent with the Fan *et al.* (2001) LF with $\beta = -2.58$ extrapolated to $z = 6.1$ (shown with "plus" signs in Figure 1). This clearly shows how the high-redshift LF is more consistent with a PDE beyond $z \sim 5$. Richards *et al.* (2006) have recently found from a sample of SDSS QSOs, that the high-redshift QSO LF bright slope flattens at $z \gtrsim 2.5$ from $|\beta'| = 3.2$ down to $|\beta'| \gtrsim 2.4$ at $z \sim 5$. We suggest instead that a double power-law, steeper at bright magnitudes and shallower at fainter ones, is more indicative for the QSO LF at $z \sim 6$. Our results on the optical LF are instead in good agreement with those by Fontanot *et al.* (2006a), who compiled the QSO LF from a sample of GOODS and SDSS QSOs in the range $3.5 < z < 5.2$. They find significant evidence for a bright-end slope of $|\beta'| = 3.3$, a break in the LF at $M_{1450}^* \sim -25$ and a strong flattening below this limit.

3.2. The Type I plus Type II AGN Luminosity Function

In the previous section we have considered the detected sources in the CDFN as Type I AGNs. The single high-redshift source detected with spectroscopic redshift of $z = 5.19$ can in fact be safely considered as a Type I AGN. Converting its measured hard X-ray flux $f_{2-8\text{ keV}} \sim 7 \times 10^{-16} \text{ erg cm}^{-2} \text{ s}^{-1}$ to optical magnitudes (using equation (3)) we get $z_{\text{AB}} \sim 23.6$, very close to its actual magnitude of $z_{\text{AB}} \sim 23.9$. However some of the nine optically faint spectroscopically unidentified objects found by Barger *et al.* (2003) could be considered moderately obscured sources, with very faint optical fluxes (though still detectable). In this section we give constraints on the faint-end shape for the AGN LF, including the CDFN spectroscopically unidentified sources assuming that a certain fraction of them are Type II AGNs lying

at $z \sim 6$.

Indeed the 2 – 8 keV band corresponds to the 14 – 56 keV intrinsic band at $z = 6$, which is not much affected by absorption for column densities $\log N_H \lesssim 24 \text{ (cm}^{-2}\text{)}$. Here we notice however that we do not expect the detection of any very obscured, Compton-thick source in the CDFN, with $\log L_{2-10 \text{ keV}} \lesssim 44 \text{ (erg s}^{-1}\text{)}$. From Wilman & Fabian (1999) we have taken the spectrum of two typical AGNs with column densities $\log N_H = 24.25 \text{ (cm}^{-2}\text{)}$ and $\log N_H = 24.75 \text{ (cm}^{-2}\text{)}$, derived from a Monte-Carlo realization which includes Compton down-scattering which reduces the intensity even in the highest bins of energy. We then computed the ratio between absorbed and unabsorbed luminosities (the former is the actual *observed* flux) for the various spectra in the $z = 6$ redshifted, restframe energy hard band 14–70 keV (the least absorbed band of the CDFN).

We find that the ratio $L_{14-70 \text{ keV}}^{\text{abs}}/L_{14-70 \text{ keV}}^{\text{unabs}}$ is $\sim 71\%$ for $\log N_H = 24.25 \text{ (cm}^{-2}\text{)}$ and $\sim 30\%$ for $\log N_H = 24.75 \text{ (cm}^{-2}\text{)}$ (to notice for comparison that an AGN with $\log N_H = 23.5 \text{ (cm}^{-2}\text{)}$ has a ratio of $\sim 96\%$). A typical source with intrinsic luminosity $L_{2-10 \text{ keV}} = 10^{44} \text{ (erg s}^{-1}\text{)}$ (fainter luminosities would be below the X-ray flux limit) in the observed frame will in turn produce observed fluxes $f_{2-8 \text{ keV}} \approx 2 \times 10^{-16} \text{ erg cm}^{-2} \text{ s}^{-1}$ and $f_{2-8 \text{ keV}} \approx 1 \times 10^{-16} \text{ erg cm}^{-2} \text{ s}^{-1}$ for respectively the $\log N_H = 24.25 \text{ (cm}^{-2}\text{)}$ and $\log N_H = 24.75 \text{ (cm}^{-2}\text{)}$ case. Therefore sources with $\log N_H \gtrsim 24 \text{ (cm}^{-2}\text{)}$ and $\log L_{2-10 \text{ keV}} \lesssim 44 \text{ (erg s}^{-1}\text{)}$, would be hardly visible in the CDFN field of view (we remind that the flux limit is $f_{2-8 \text{ keV}} \approx 2 \times 10^{-16} \text{ erg cm}^{-2} \text{ s}^{-1}$).

On the other hand moderately obscured sources (with $\log N_H \lesssim 24 \text{ (cm}^{-2}\text{)}$) would definitely be visible at these high redshifts, and some of them might have been already discovered in the deep *Chandra* fields, among the optically faint Barger *et al.* (2003) sample. Other possible indications of the presence of Type II sources in the high redshift universe also come from Koekemoer *et al.* (2004). From the 2 msec Hubble Deep Field-North and the 1 msec CDFS, these authors have robustly detected a sample of seven sources with extreme optical/X-ray flux ratios > 10 at a flux limit above $f_{0.5-8 \text{ keV}} \approx 3 \times 10^{-16} \text{ erg cm}^{-2} \text{ s}^{-1}$. Although these kind of sources are generally rare, if they are AGNs lying at $z > 6$ such that their Ly α

emission has been redshifted out of the z_{AB} band-pass, then they would definitely be high-redshift obscured sources. We cannot directly make a prediction with their data as we are converting to optical luminosities and these are special sources, strong outliers with respect to equation (3) (also a conversion to bolometric luminosity would be difficult in this case).

In this section we still adopt the same X-ray K -correction as for unabsorbed sources with $\Gamma = 1.8$ to convert flux to luminosities. We still use equation (3), which holds for Type I AGNs, for converting X-ray fluxes to intrinsic optical luminosities for Type II AGNs, assuming that unification models are on average valid. First we consider *all* the sources detected by Barger *et al.* (2003) as optically faint Type II AGNs lying at $z > 5$. We then integrate equation (6) in the redshift range $5 \lesssim z \lesssim 6.5$ above a flux limit of $f_{2-8 \text{ keV}} = 2 \times 10^{-16} \text{ erg cm}^{-2} \text{ s}^{-1}$ corresponding to an effective area of 40 arcmin² (see Figure 19, bottom panel in Alexander *et al.* 2003). The adopted flux limit corresponds to apparent magnitudes $z_{\text{AB}} > 25.5$ at $z \sim 5.7$ (equation (3)). Using $\beta = 3.45$ we obtain ~ 9 sources in the field of view, corresponding to a comoving density of $\log[dn/dM(-21.2, 5.7)] \sim -3.85 \text{ Mpc}^{-3} \text{ mag}^{-1}$.

The results are shown with an open square with its 99% confidence level in Figure 2 with its error bar on the optical luminosity when using equation (3). If the nine sources are confirmed to be Type II AGNs at $z \sim 6$, this would show evidence for an extraordinary contribution of Type II AGNs at the faint end of the AGN LF. Assuming all these faint sources to lie at $z \sim 6$ would imply a fraction obscured-to-unobscured AGNs of order 9. X-ray surveys at lower redshifts found much more moderate numbers for this ratio (e.g. Ueda *et al.* 2003, La Franca *et al.* 2005, Gilli *et al.* 2006).

In fact the above scenario is an extreme one, as most probably many of these optically faint sources probably belong to lower redshifts (see discussions in Barger *et al.* 2003 and Cowie *et al.* 2003). Therefore we more safely assume that up to 3 sources, out of the 9 detected, i.e. three times the surface density of the Type I LF (made up of only the single $z = 5.19$ source), are actual contributors to $z \sim 6$ AGN LF with $\log N_H \lesssim 24 \text{ cm}^{-2}$, following the results by La Franca *et al.* (2005), who find an almost flat distribution

of the fraction of sources per logarithm bin of N_H . In this second case we get a comoving density of $\log[dn/dM(-21.2, 5.7)] \sim -4.3 \text{ Mpc}^{-3} \text{ mag}^{-1}$, shown as a solid square in Figure 2 with its 99% CL error bars.

We then compare our AGN LF estimate with what would be obtained by multiplying the average QSO LF (with a faint slope of $\beta = -2.5$; section 3.1) by a factor $1 + R$, where R is the ratio between Type II and Type I AGNs, as calibrated by several groups for AGNs detected at lower redshifts. For computing R we also include sources up to $\log N_H \lesssim 26 \text{ cm}^{-2}$. We use the results by Ueda *et al.* (2003), La Franca *et al.* (2005) and Gilli *et al.* (2006). As specified above, we consider Type II AGNs all those sources with $\log N_H > 22 \text{ cm}^{-2}$. Therefore by definition the number ratio Type II-to-Type I will be given by $R = n[22 < \log(N_H/\text{cm}^{-2}) < 26]/n[\log(N_H/\text{cm}^{-2}) < 22]$. For Ueda *et al.* (2003) and La Franca *et al.* (2005) we use their quoted distributions for the fraction of objects up to $\log N_H = 26 \text{ (cm}^{-2})$.

Gilli *et al.* (2006) developed an updated model for the synthesis of the X-ray background, for which they adopted a different definition for the number ratio between obscured and unobscured AGNs, i.e. $R = n[21 < \log(N_H/\text{cm}^{-2}) < 24]/n[\log(N_H/\text{cm}^{-2}) < 21]$. According to their model this ratio is redshift-independent, luminosity-dependent and, translated to optical magnitudes, it reads as

$$R(M_{1450}) = R_s \times \exp\left(-10^{-0.4(M_{1450}-M_c)}\right) + R_q \times \left(1 - \exp\left(-10^{-0.4(M_{1450}-M_c)}\right)\right), \quad (7)$$

with $R_s = 3.6$, $R_q = 1$ and $M_c = -20.7$, i.e. $\log L_{0.5-2 \text{ keV}} \sim 43.5 \text{ (erg s}^{-1})$, where R_s and R_q are the $n[21 < \log(N_H/\text{cm}^{-2}) < 24]/n[\log(N_H/\text{cm}^{-2}) < 21]$ ratio at the low- and high-luminosity regimes respectively, and $M_c = -20.7$ is the characteristic luminosity dividing the two regimes (Gilli *et al.* 2006). To include also Compton-thick sources with column densities up to $\log N_H = 26 \text{ (cm}^{-2})$, we consider double this ratio (see Figure 7 in Gilli *et al.* 2006).

The resulting AGN LF from the Gilli *et al.* (2006) model is shown with a dashed line in Figure 2. In the same figure we also plot the results of using R as calibrated from Ueda *et al.* (2003; dot-dashed line) and La Franca *et al.* (2005; long-

dashed line). All the models for the distribution of sources as a function of N_H considered provide similar estimates for the total AGN LF, and are consistent with the extrapolated data at the faint end, when using 3 sources as proxy for the $z \sim 6$ AGN population within the effective area. We remind here that our estimate for the faint-end AGN LF could easily be underestimated, as the CDFN cannot detect Compton-thick sources (those with $\log N_H > 24 \text{ cm}^{-2}$).

To notice that all the models also provide a significant number of sources at the bright end of the AGN LF in excess of the QSO LF. Due to the small volume probed by the CDFN we however cannot provide any kind of constraint on the actual contribution of intrinsically very luminous and more rare obscured sources. Anyway in the following we will consider as our best estimate of the total AGN LF at $z \sim 6$, the QSO LF multiplied by $(1 + R_{\text{Ueda}})$, where R_{Ueda} is the Type II-to-Type I ratio as extracted from Ueda *et al.* (2003). In the following section we will compare theoretical models with such a determination of the AGN LF.

4. Implications

The high redshift AGN LF is a very sensitive tool to probe the connections between supermassive black holes (SMBHs) and their host dark matter (DM) halos. In this section we discuss possible physical implications for SMBH evolution from our estimated AGN LF. We compute the *total* AGN LF from the formation rates of DM halos simply as (e.g., Mahmood *et al.* 2005)

$$\Phi(L_B, z) \simeq t_{\text{AGN}} \times R_{\text{MM}}(M_{\text{halo}}, z) \times \frac{dM_{\text{halo}}}{dM_{\bullet}} \frac{dM_{\bullet}}{dL_B}. \quad (8)$$

Here $R_{\text{MM}}(M_{\text{halo}}, z)$ is the formation rate of DM halos with mass M_{halo} at redshift z , massive and virialized enough to host a galaxy/AGN; t_{AGN} in this model is the average timescale during which an AGN is active (but not necessarily visible). We neglect any dependence on mass for this timescale and just set it equal to $t_{\text{AGN}} = 10^7 \text{ yr}$. M_{\bullet} is the SMBH mass producing the luminosity L_B . In the following for simplicity we will use extended Press-Schechter (EPS) theory to compute $R_{\text{MM}}(M_{\text{halo}}, z)$ and we will consider only halos $\log M_{\text{halo}}/M_{\odot} \leq 13.2$. The limiting mass of $M_{\text{halo}} \sim 10^{13} M_{\odot}$ as host for the most massive

galaxies and most luminous quasars has been constrained through clustering (e.g. Croom *et al.* 2005), statistical (e.g. Shankar *et al.* 2006), and semi-analytical (e.g. Granato *et al.* 2004) techniques.

Most probably the EPS theory is a rather poor approximation for describing the statistics of high redshifts AGN host halos, moreover a more physical treatment of the baryonic processes is required when comparing with observations (e.g. Lapi *et al.* 2006, Fontanot *et al.* 2006b). However here we neglect such issues and focus on the most suitable relation $M_\bullet - M_{\text{halo}}$, among those suggested in the literature, which better compares with observations within the very basic model expressed in equation (8). We therefore consider different recipes for the jacobian relation in equation (8) relating DM and SMBH mass.

We first discuss the Wyithe & Loeb (2003; see also Mahmood *et al.* 2005) model which connects the SMBH and DM halo masses as $M_\bullet \propto M_{\text{halo}}^{5/3}(1+z)^{5/2}$, derived from a basic AGN feedback-constrained model. We shall refer to this model as model A in the rest of the paper. Using Model A, we calculate the $z = 6.1$ LF, shown as a solid line in Figure 3. This model is consistent with the AGN LF estimated in section 3.2.

Several other groups have also formulated theoretical models for describing SMBH evolution in the context of cosmological theories (e.g. Haenelt & Rees 1993, Cavaliere & Vittorini 2000, Vittorini *et al.* 2005, Hopkins *et al.* 2005). Here we adopt a simple version of one of these models, viz. the model by Kauffmann & Haenelt (2000; see also Croton 2005) who parameterize the link between SMBH mass and halo mass as:

$$M_\bullet = 0.03m_R \left[1 + \left(\frac{280 \text{ km s}^{-1}}{V_{\text{vir}}} \right)^2 \right]^{-1} m_{\text{cold}}, \quad (9)$$

where m_R represents the merger mass ratio between the central and satellite galaxies, i.e. $m_R = m_{\text{sat}}/m_{\text{central}}$, V_{vir} is the virial velocity of the AGN host halo and m_{cold} is the amount of cold baryonic matter (which will eventually form stars). The equation (9) prescription with $m_R = 1$, consisting of only major mergers, is our model B.

We then consider three cases in which the cold fraction is $m_{\text{cold}} = 0.1 \times M_{\text{halo}}$, $m_{\text{cold}} = 0.016 \times M_{\text{halo}}$, and $m_{\text{cold}} = 0.005 \times M_{\text{halo}}$. The result-

ing LFs are plotted in Figure 4. The first case, in which the amount of baryons per halo is close to the cosmological value, lies well above the observed LF. The second case fits the bright-end LF, assuming a baryonic fraction of a few percent, consistent with results by Shankar *et al.* (2006). It is interesting to note that a strong decrease of baryonic mass fraction with decreasing halo mass is needed to reproduce the AGN LF, down to only 0.5% at the very faint end.

We now test a model based on Ferrarese *et al.* (2002; see also Shankar *et al.* 2006). We call this model C, and is the most empirical way to track the $M_\bullet - M_{\text{halo}}$ relation. We relate the SMBH mass to bulge velocity dispersion using the $M_\bullet - \sigma$ relation. The σ is then connected to the circular velocity of the host galaxy by using the empirical $\sigma - V_C$ relation (from Baes *et al.* 2003). The circular velocity is then scaled to the virial velocity assuming a Navarro, Frenk & White (1996; NFW) profile and a concentration parameter $c(M_{\text{halo}}, z)$ from Bullock *et al.* (2001). Finally the virial velocity is converted to halo mass using the virial theorem, $GM_{\text{halo}}/R_{\text{vir}} = V_{\text{vir}}^2(z_{\text{vir}})$ (we use the relations in Loeb & Peebles 2003 given for each z_{vir}), which is computed at the moment of the virialization of the host DM halo (i.e. we set $z_{\text{vir}} = 6.1$). We also add a scatter of ~ 0.35 in the resulting $M_\bullet - M_{\text{halo}}$ relation, as empirically suggested by Ferrarese (2002) and theoretically supported by Lapi *et al.* (2006). Our result reads as

$$M_\bullet = 5.8 \times 10^7 \left(\frac{M_{\text{halo}}}{10^{12} M_\odot} \right)^{1.39} \left(\frac{1+z}{7} \right) M_\odot, \quad (10)$$

which is close to the one calibrated locally through statistical arguments by Shankar *et al.* (2006) and to the one obtained by Granato *et al.* (2004) and Lapi *et al.* (2006) in semi-analytical models.

One uncertainty in the above computations is the radius at which one measures the circular velocity. Ferrarese (2002) uses $R \sim R_s$ (also used in equation 10), where R_s is the scale radius of the NFW DM profile. In Figure 5 we compare the predictions of model C with the calibrated high- z AGN LF. The model matches the data when $R \sim (0.5 - 1)R_s$ and it has the advantage of being empirically-based, the only assumption here is that the $M_\bullet - \sigma$ and $\sigma - V_c$ relations are almost constant in time.

Our findings therefore differ from those in Willott *et al.* (2005b), who attempted a similar calculation and found that the number of DM halos at $z \sim 6$ falls short by several orders of magnitude in accounting for the number of high-redshift AGNs. Their conclusions were based on the use of the virial theorem calibrated at $z_{\text{vir}} = 0$, which inevitably leads to significantly underestimating the BH mass (and therefore AGN luminosity) for a given halo. Our findings are consistent with $\sigma \sim (0.5 - -0.6)V_{\text{vir}}(M_{\text{halo}}, z)$. The latter relation in turn has been used by Cirasuolo *et al.* (2005) to show that an impressive fit to the dispersion velocity function (Sheth *et al.* 2003; Shankar *et al.* 2004) is recovered when integrating the DM formation rates $R_{MM}(M_{\text{halo}}, z_{\text{vir}})$ and setting $\sigma \sim 0.57 \times V_{\text{vir}}(M_{\text{halo}}, z_{\text{vir}})$ (see also Loeb & Peebles 2003 and Shankar *et al.* 2006).

The simple approach undertaken in this section shows that a, redshift-dependent, super-linear relation of the type $M_{\bullet} \propto M_{\text{halo}}^{\alpha}$, with $1.3 \lesssim \alpha \lesssim 1.7$, as the ones proposed in model A and C, is best suited to represent the AGN LF determined in section 3.2. Alternative scenarios would require a very strong variation of baryonic content and/or AGN activity timescale with halo mass.

5. Contribution to Reionization

In this section we compute the possible contribution of AGNs and stars to the reionization of the universe. In the following we will consider only Type I AGNs as contributors of the reionization along our line of sight. The transition from a neutral to a fully ionized Inter Galactic Medium (IGM) is usually statistically described by a differential equation for the time evolution of the volume filling factor of the medium $Q(z)$. The latter quantity quantifies the level of the IGM *porosity* created by the HII, HeII and HeIII ionization regions around radiative sources such as QSOs and galaxies.

When the clumping factor of the medium is high, $C \gg 1$, which is always a good approximation at high redshifts (the simulations by Gnedin & Ostriker 1997 give $C \sim 30$), following Madau *et al.* (1999) one can approximate $Q(t) \approx \dot{n}_{\text{ion}}/\bar{n}_H \bar{t}_{\text{rec}}$, where \bar{t}_{rec} is the volume-averaged mean recombination rate, \dot{n}_{ion} is the total rate of ionizing photons and \bar{n}_H is the mean

hydrogen density of the expanding IGM.

The condition for reionization will then read $Q \approx 1$, which translates into a total required ionizing photon rate (Madau *et al.* 1999; Fan *et al.* 2001):

$$\dot{n}_{\text{ion}}(z) = 10^{51.2} \left(\frac{C}{30} \right) \left(\frac{1+z}{6} \right)^3 \left(\frac{\Omega_b h_{0.5}^2}{0.08} \right)^2. \quad (11)$$

We compare such a rate with those from QSOs and galaxies at similar redshifts. We start computing the photoionization rate from QSOs, which is given by (e.g. Madau *et al.* 1999, Stiavelli *et al.* 2004)

$$\dot{n}_{\text{AGN}} = \int_{\nu_H}^{\infty} \frac{E(\nu)}{h_P \nu} d\nu, \quad (12)$$

where h_P is the Planck's constant, $\nu_H = 3.2 \times 10^{15}$ Hz is the frequency at the Lyman limit (912 Å, i.e. one Rydberg). The volume emissivity of the total population of sources is given as

$$E(\nu) = \int_{L_{\text{min}}}^{\infty} \Phi(L, z) L_{\nu}(L) dL, \quad (13)$$

where L_{ν} is in $\text{erg s}^{-1} \text{Hz}^{-1}$. The integration in equation (12) is usually performed up to 4 Rydbergs, as photons more energetic than that are preferentially absorbed by He atoms. Anyway we have checked that extending the computation to ~ 40 Rydbergs for example, increases our final results by just $\sim 12\%$. L_{min} in equation (13) is instead the minimum luminosity probed by the survey, which we fix to $M_{1450} = -20.6$, following the results in section 3.1.

We thus find that the AGN contribution to reionization at redshift $z \sim 6$ integrating down to $M_{1450} = -20.6$, varies from 2% to $\sim 9\%$, using a faint-end slope β of -2.2, -2.8 respectively. These results are rather independent of the details for the AGN spectrum. For the computations above we have used the spectrum described in Schirber & Bullock (2003), however using, for example, the three-power law spectrum adopted by Madau *et al.* (1999), reduces the AGN contribution by $\lesssim 13\%$.

We follow Meiksin (2005) for computing the photoionization rate from galaxies

$$\dot{n}_{\text{Galx}} = f_{\text{esc}} \frac{dN_{\text{phot}}}{dM_{\text{star}}} \rho_{\text{star}}. \quad (14)$$

Here $dN_{\text{phot}}/dM_{\text{star}} \approx 10^{61} \text{ phot s}^{-1}$ is the production rate of ionizing photons per solar mass of stars formed, ρ_{star} is the Star Formation Rate (SFR) in units of $M_{\odot} \text{ yr}^{-1} \text{ Mpc}^{-3}$, and f_{esc} is the average fraction of ionizing photons which can freely escape the star-forming regions into the IGM.

The photons per solar mass has been taken from Smith *et al.* (2002; see also Meiksin 2005) for a Salpeter Initial Mass Function (IMF) and a metallicity of 20% the solar. The SFR was instead recently derived by Richard *et al.* (2006) to be $\sim 0.027 M_{\odot} \text{ yr}^{-1} \text{ Mpc}^{-3}$ from a deep survey of lensing clusters aimed at constraining the abundance of star-forming galaxies at redshift $z \sim 6 - 10$. We then take results from the recent paper by Shapley *et al.* (2006), who have constrained the escape fraction in the ionizing Lyman continuum from a sample of 14 $z \sim 3$ star-forming galaxies, finding an average $f_{\text{esc}} \sim (11 - 18)\%$, and we use the average value of $f_{\text{esc}} \sim 15\%$. In the following we neglect the diffuse emission from the IGM itself which however could add an additional photoionization rate (up to 50%, e.g. Meiksin & Madau 1993) over the direct one from the sources. We find that galaxies can contribute about 50% at $z = 6.1$ to reionization.

We now take a step forward and integrate the contribution to reionization from both type of sources within the range of the *Chandra* deep fields, i.e. $5.5 \lesssim z \lesssim 6.5$, and compare the inferred number of ionizing photons with the number of available neutral hydrogen atoms at $z \sim 6$, $n_H = 6.2 \times 10^{66}$ (see Stiavelli *et al.* 2004). We find that the contribution from AGNs to grow up to $(7 - 30)\%$ while the one from galaxies being about 70%, keeping the SFR constant in this redshift bin, as suggested by observations. The PDE evolution of the AGN LF for $z < 6$ makes the contribution from AGNs grow more than the one from galaxies.

The photons produced by galaxies reach an average contribution to reionization of $\gtrsim 70\%$, implying a minor contribution from QSOs, a conclusion in very good agreement with previous calculations (e.g. Meiksin 2005, Fan *et al.* 2001, Barger *et al.* 2003). However we also notice that Bouwens *et al.* (2005) from the deep NICMOS fields in the Hubble Ultra Deep Fields (HUDF) have detected 5 objects in 5.7 sq. deg., inferring a SFR about a factor of 2 – 3 below the one found by Richard

et al. (2006). This would drop the galaxy contribution down to $(25 - 40)\%$. Similar points were also recently addressed by Mannucci *et al.* (2006) who claim that the high-redshift SFR could fall short of completely reionizing the universe. They however also point out that the Bouwens *et al.* (2005) estimate should be further increased by a factor of 2 for dust extinction and/or accounting for luminosity evolution in the estimate. Using therefore the Bouwens *et al.* (2005) result in equation (14) would still leave room for a significant contribution from QSOs. Other ways to fill the possible "missing" photons from galaxies could be to alter significantly the photon luminosity from massive stars, invoking extra IGM diffuse light, or including other photoionizing sources (such as Population III stars and/or miniquasars powered by intermediate-mass BHs). However the contribution from the latter sources must be $\lesssim 30\%$ at the most.

6. Conclusions

In a recent paper, Cool *et al.* (2006) found three QSOs at high redshifts ($z > 5.4$) down to magnitudes of $M_{1450} \sim -26.7$. The detection of these quasars is roughly consistent with the extrapolation of the bright steep slope of the quasar LF by F04 with $\beta = -3$. At lower magnitudes not many QSOs are observed, as recently concluded by the optical/NIR surveys conducted by M05, Stern *et al.* (2005) and Willott *et al.* (2005). In this paper we show that such *non*-detection of QSOs implies a significant downturn in the optical QSO LF at lower magnitudes with respect to those probed by Cool *et al.* (2006). Moreover we show that the *Chandra* deep field observations probe about 1 – 2 magnitudes deeper than the optical ones (down to $M_{1450} = -20.6$). The inferred faint end co-moving number density is lower by at least an order of magnitude with respect to the extrapolation of the F04 LF, at a high significance level.

If a fraction of the nine *Chandra* deep field sources are Type II AGNs detected at X-ray fluxes $f_{2-8 \text{ keV}} \gtrsim 2 \times 10^{-16} \text{ erg cm}^{-2} \text{ s}^{-1}$ and with very faint optical magnitudes ($z_{\text{AB}} > 25.2$), this would place a constraint on the shape of the Type I plus Type II AGNs at faint magnitudes, being consistent with a slope close to the extrapolation of the F04 LF, i.e. $|\beta| \gtrsim 3$. This estimate of the AGN LF

is however representative of only the sources with $\log N_H \sim 24 (\text{cm}^{-2})$, as more obscured sources would be below the CDFN flux limit. X-ray surveys at lower redshifts (e.g. La Franca et al. 2005) have shown that an almost flat distribution in the number of sources is observed up to column densities of $\log N_H \sim 24 (\text{cm}^{-2})$. We can therefore safely assume that only 3, out of the nine optically faint sources to be AGNs at $z \sim 6$. This yields a total AGN LF consistent with updated synthesis models for the XRBG.

We then compare this result with predictions from three simple physically and empirically motivated basic models for AGN evolution in DM halos. We generally find that a redshift-dependent relation of the kind $M_\bullet - M_{\text{halo}}^\alpha$, with $1.3 \lesssim \alpha \lesssim 1.7$, produces models more consistent with the AGN LF. Such relations were also found from independent statistical studies by Shankar *et al.* (2006) and rotation curve extrapolations in spirals and ellipticals (Ferrarese 2002). Alternative models, such as varying the amount of cold gas fraction or AGN active timescale in smaller halos, would require extreme fine tuning and a large variation in the parameters with dark matter halo mass. Here we also notice that if we reduce the AGN duty-cycle just to the visible optical phase, i.e. substituting t_{AGN} with t_{QSO} in equation (6), the match between models and the Type I AGN LF derived in section 3.1, would yield similar results on the type of $M_\bullet - M_{\text{halo}}$ relation.

Finally we have shown that AGNs can account for at most 30% of the total reionization of the Universe at redshifts around $z \sim 6$. However we also notice that a strong caveat on the actual role of galaxies in reionizing the universe, is set by the normalization of the cosmological SFR at high redshifts, which is still uncertain by factors of about 2.

We acknowledge C. S. Kochanek, P. S. Osmer, D. Weinberg and P. Martini for helpful discussions. FS also acknowledges S. Cristiani and F. Fontanot for sharing data on the quasar template spectrum. The authors are highly indebted to the referee for his/her very useful comments and suggestions. This work was supported in part by NASA grant GRT000001640.

REFERENCES

- Alexander, D. M., et al. 2003, *AJ*, 126, 539
- Baes, M., Buyle, P., Hau, G. K. T., & Dejonghe, H. 2003, *MNRAS*, 341, L44
- Barger, A. J., et al. 2003, *AJ*, 126, 632
- Boyle, B. J., et al. 1991, in *ASP Conf. Ser. 21, The Space Distribution of Quasars*, ed. D. Cramp-ton (San Francisco: ASP), 191
- Brandt, W. N. et al. 2002, *ApJ*, 569, L5
- Bullock, J. S., Kolatt, T. S., Rachel, Y. S., Somerville, S., Kravtsov, A. V., Klypin, A. A., Primack, J. R., & Dekel, A. 2001, *MNRAS*, 321, 559
- Cavaliere, A., & Vittorini, V. 2000, *ApJ*, 543, 599
- Cimatti, A., et al. 2002, *A&A*, 392, 395
- Cirasuolo, M., Shankar, F., Granato, G. L., De Zotti, G., & Danese, L. 2005, *ApJ*, 629, 816
- Cool, R. J., Kochanek, C. S., Eisenstein, D. J., Stern, D., Brand, K., Brown, M. J. I., Dey, A., Eisenhardt, P. R., Fan, X., Gonzalez, A. H., Green, R. F., Jannuzi, B. T., McKenzie, E. H., Rieke, G. H., Rieke, M., Soifer, B. T., Spinrad, H., & Elston, R. J. 2006, *AJ*, in press, [astroph/0605030](#)
- Cowie, L. L., et al. 1995, *Nature*, 377, 603
- Cowie, L. L., et al. 2002, *ApJ*, 566, L5
- Cowie, L. L., et al. 2003, *ApJ*, 584, L57
- Cristiani, S., & Vio, R. 1990, *A&A*, 227, 385
- Cristiani, S., et al. 2004, *ApJ*, 600, L119
- Croom, S. M., et al. 2005, *MNRAS*, 356, 415
- Croton, D. J. 2005, [astroph/0512375](#)
- Dijkstra, M., & Wyithe, J. S. B. 2006, [astroph/0606334](#)
- Fan, X., et al. 2001, *AJ*, 121, 54
- Fan, X., et al. 2001b, *AJ*, 122, 2833
- Fan, X., et al. 2004, *ApJ*, 128, 515

- Ferrarese, L. 2002, *ApJ*, 578, 90
- Ferrarese, F., & Ford, H. C. 2005, *SSRv*, 116, 523
- Fiore, F., et al. 2003, *A&A*, 409, 79
- Fontanot, F., Cristiani, S., Monaco, P., Nonino, M., Vanzella, E., Brandt, W. N., Grazian, A., & Mao, J. 2006a, *A&A*, accepted, [astroph/0608664](#)
- Fontanot, F. S., Monaco, P., Cristiani, S., & Tozzi, P. 2006b, *MNRAS*, accepted, [astroph/0609823](#)
- Gehrels, N. 1986, *ApJ*, 303, 336
- Gilli, R., Comastri, A., & Hasinger, G. 2006, *A&A*, accepted, [astroph/0610939](#)
- Granato, G. L., Silva, L., Monaco, P., Panuzzo, P., Salucci, P., De Zotti, G., & Danese, L. 2001, *MNRAS*, 324, 757
- Granato, G. L., De Zotti, G., Silva, L., Bressan, A., & Danese, L. 2004, *ApJ*, 600, 580
- Haehnelt, M. G., Rees, M.J. 1993, *MNRAS*, 263, 168
- Hopkins, P. F., Hernquist, L., Cox, T. J., Di Matteo, T., Robertson, B., & Springel, V. 2005, *ApJS*, in press ([astroph/0506398](#))
- Kauffmann, G., & Haehnelt, M. 2000, *MNRAS*, 311, 576
- Kennefick, J. D., Djorgovski, S. G., & de Carvalho, R. R. 1995, *AJ*, 110, 2553
- La Franca, F., et al. 2005, *ApJ*, 635, 864
- Lapi, A., Shankar, F., Mao, J., Granato, G. L., Silva, L., De Zotti, G., & Danese, L. *ApJ*, in press, [astroph/0603819](#)
- Loeb, A., & Peebles, P. J. E. 2003, *ApJ*, 589, 29
- Mahabal, A., Stern, D., Bogosavljevic, M., Djorgovski, S.G., & Thompson, D. 2005, *ApJ*, 634, L9
- Mahmood, A., Devriendt, J. E. G., & Silk, J. 2005, *MNRAS*, 359, 1363
- Mannucci, F., Buttery, H., Maiolino, R., Marconi, A., & Pozzetti, L. 2006, [astroph/0607143](#)
- Mathur, S., Wilkes, B. J., & Ghosh, H. 2002, *ApJ*, 570, L5
- Monaco, P., Salucci, P., & Danese, L. 2000, *MNRAS*, 311, 279
- Navarro, J. F., Frenk, C. S., & White, S. D. M. 1997, *ApJ*, 490, 493 (NFW)
- Osmer, P. S. 2004, in Ho L.C., ed., *Carnegie Observatories Astrophysics Series, Vol. 1, Coevolution of Black Holes and Galaxies*. Cambridge Univ. Press, Cambridge, p. 324
- Pei, Y. C. 1995, *ApJ*, 438, 623
- Richards, G. T., et al. 2005, *MNRAS*, 360, 839
- Richards, G. T., et al. 2006, *AJ*, in press ([astroph/0601434](#))
- Shankar, F., Salucci, P., Granato, G. L., De Zotti, G., & Danese, L. 2004, *MNRAS*, 354, 1020
- Shankar, F., Lapi, A., Salucci, P., De Zotti, G., & Danese, L. 2006, *ApJ*, 643, 14
- Shapley, A. E., Steidel, C. C., Pettini, M., Adelberg, K. L., & Erb, D. K. 2006, *ApJ* in press, [astroph/0606635](#)
- Sharp, R. G., Crampton, D., Hook, I. M., & McMahon, R. G. 2004, *MNRAS*, 350, 449
- Sheth, R. K., & Tormen, G. 2002, *MNRAS*, 329, 61L
- Schirber, M., & Bullock, J. S. 2003, *ApJ*, 584, 110
- Spergel, D. N., et al. 2003, *ApJS*, 148, 175
- Springel, V., et al. 2005, *Nature*, 435, 629
- Schmidt, M, Schneider, D. P., & Gunn, J. E. 1995, *AJ*, 110, 68
- Steffen, A. T., Strateva, I., Brandt, W. N., Alexander, D. M., Koekemoer, A. M., Lehmer, B. D., Schneider, D. P., & Vignali, C. 2006, *AJ*, 131, 2826
- Stern, D., et al. 2000, *ApJ*, 533, L75
- Stern, D., et al. 2000b, *AJ*, 119, 1526
- Stiavelli, M., Fall, S. M., & Panagia, N. 2004, *ApJ*, 600, 508

- Tezca, M., et al. 2004, ApJ, 605, L109
- Ueda, Y., Akiyama, M., Ohta, K., & Miyaji, T. 2003, ApJ, 598, 886
- Vignali, C., Brandt, W. N., & Schneider, D.P. 2003, AJ, 125, 433
- Vittorini, V., Shankar, F., & Cavaliere, A. 2005, MNRAS, 363, 1376
- Willott, C. J., Delfosse, X., Forveille, T., Delorme, P., & Gwyn, S. D. J. 2005, ApJ, 633, 630
- Willott, C. J., et al. 2005b, ApJ, 626, 657
- Wilman, R. J., & Fabian, A. C. 1999, ApJ, 309, 862
- Wolf, C., et al. 2003, A&A, 408, 499
- Wyithe, J. S. B. 2004, MNRAS, 351, 1266
- Wyithe, J. S. B., & Loeb, A. 2003, ApJ, 595, 614

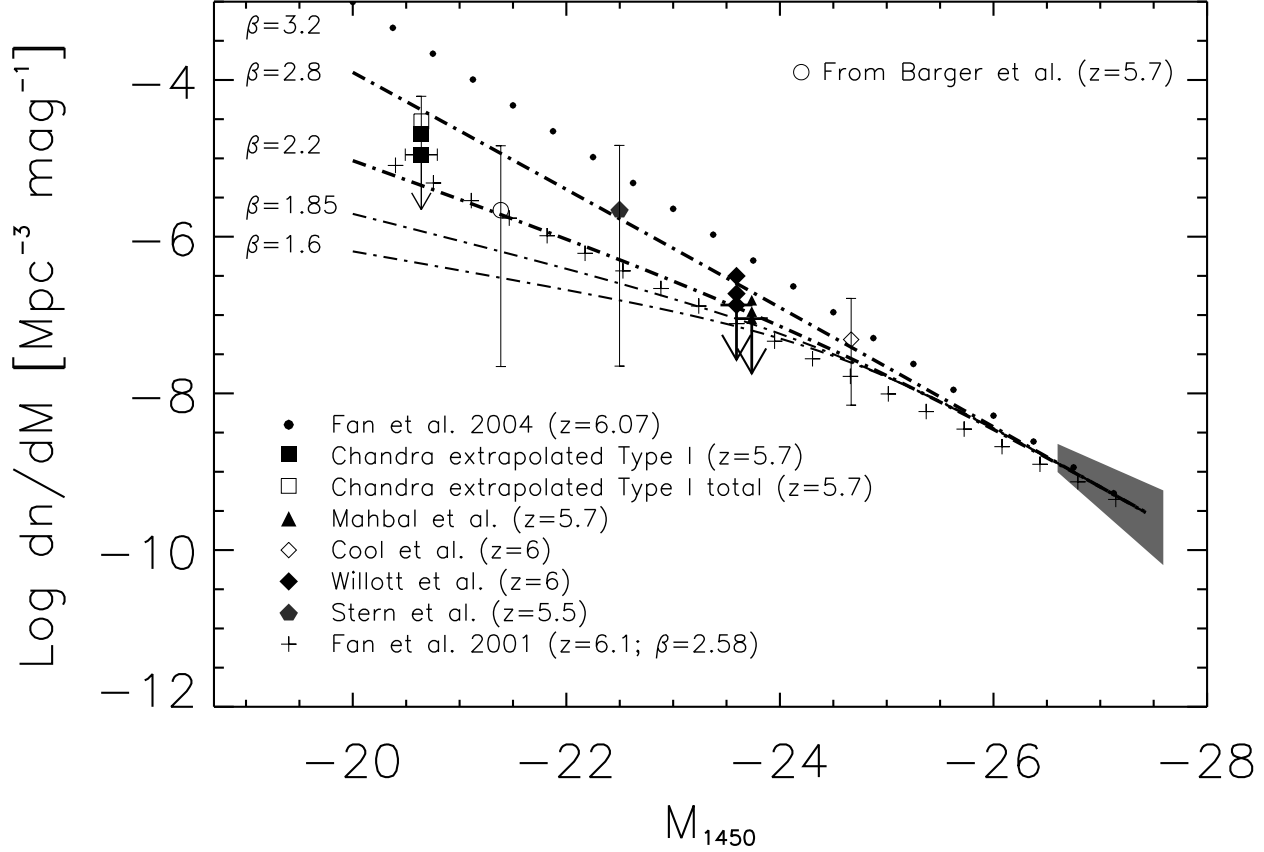


Fig. 1.— Type I AGN Luminosity Function at $z \sim 6$. The *squares* represent the estimated AGN density at the optical magnitude of $M_{1450} \sim -20.6$ needed for a single source to be detected above the broad band X-ray flux limit of $f_{0.5-8 \text{ keV}} \approx 2.5 \times 10^{-16} \text{ erg cm}^{-2} \text{ s}^{-1}$ in 160 arcmin^2 . From top to bottom the two *solid squares* are the 99% and 90% confidence level estimates, while the *open square* has been estimated taking into account all the nine spectroscopically unidentified sources in the deep *Chandra* fields with its 99% error bars; the horizontal error bar reflects the uncertainty in the computation of the optical magnitude at fixed X-ray flux when the $1-\sigma$ uncertainty in equation (3) are taken into account. The *open circle* is the AGN luminosity function estimated from Barger *et al.* (2003) with its 99% CL. The *solid pentagon* is the AGN density from Stern *et al.* (2000) with the 99% confidence level error bars; the *solid diamonds* are the AGN densities from Willott *et al.* (2005) again shown with 99%, 95% and 90% confidence level (from top to bottom); the *solid triangles* are the AGN densities computed from Mahabal *et al.* (2005), with 99%, 95% and 90% confidence level (from top to bottom); the *open diamond* is the AGN density computed from Cool *et al.* (2006) with its 99% confidence level error bars; the *crosses* are the Fan *et al.* (2001) luminosity function extrapolated to $z = 6.1$ assuming PDE from $z = 5$. The values reported on the upper-left of the figure are the absolute values for the faint slopes of the model AGN luminosity function in equation (6); the *shaded area* is the observed luminosity function by Fan *et al.* (2004) with its $1-\sigma$ uncertainty while the *thick-dotted line* is its extrapolation to fainter magnitudes.

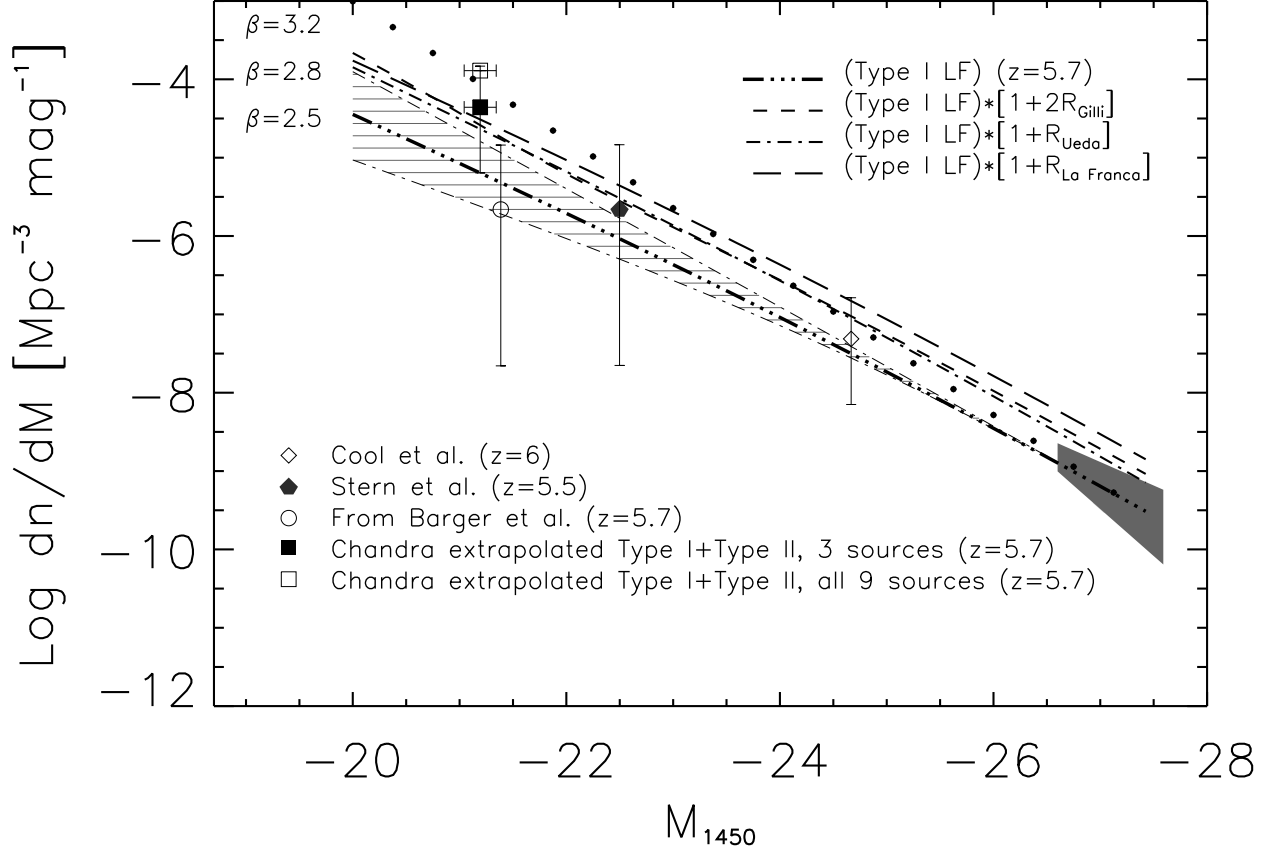


Fig. 2.— Type I plus Type II AGN luminosity function. The *open square* is the AGN luminosity function considering all the nine sources in the *Chandra* deep fields as Type II AGNs; the *solid square* is instead the AGN luminosity function computed when 3 sources are taken from the Barger *et al.* (2003) optically faint sample to be $z \sim 6$ AGN candidates. The *triple dot-dashed* line is the Type I AGN luminosity function with the average slope of $\beta = -2.5$ and the *striped area* is the range of 90–99% CL for the Type I AGN luminosity function; the *dashed* line is the Type I AGN luminosity function multiplied by $1 + 2R$ where R is the Type II/Type I ratio as given in Gilli *et al.* (2006; equation (8)), while in the *dot-dashed* and *long-dashed* lines R has been extracted from Ueda *et al.* (2003) and La Franca *et al.* (2005) respectively. All the other symbols and lines are as in Figure 1.

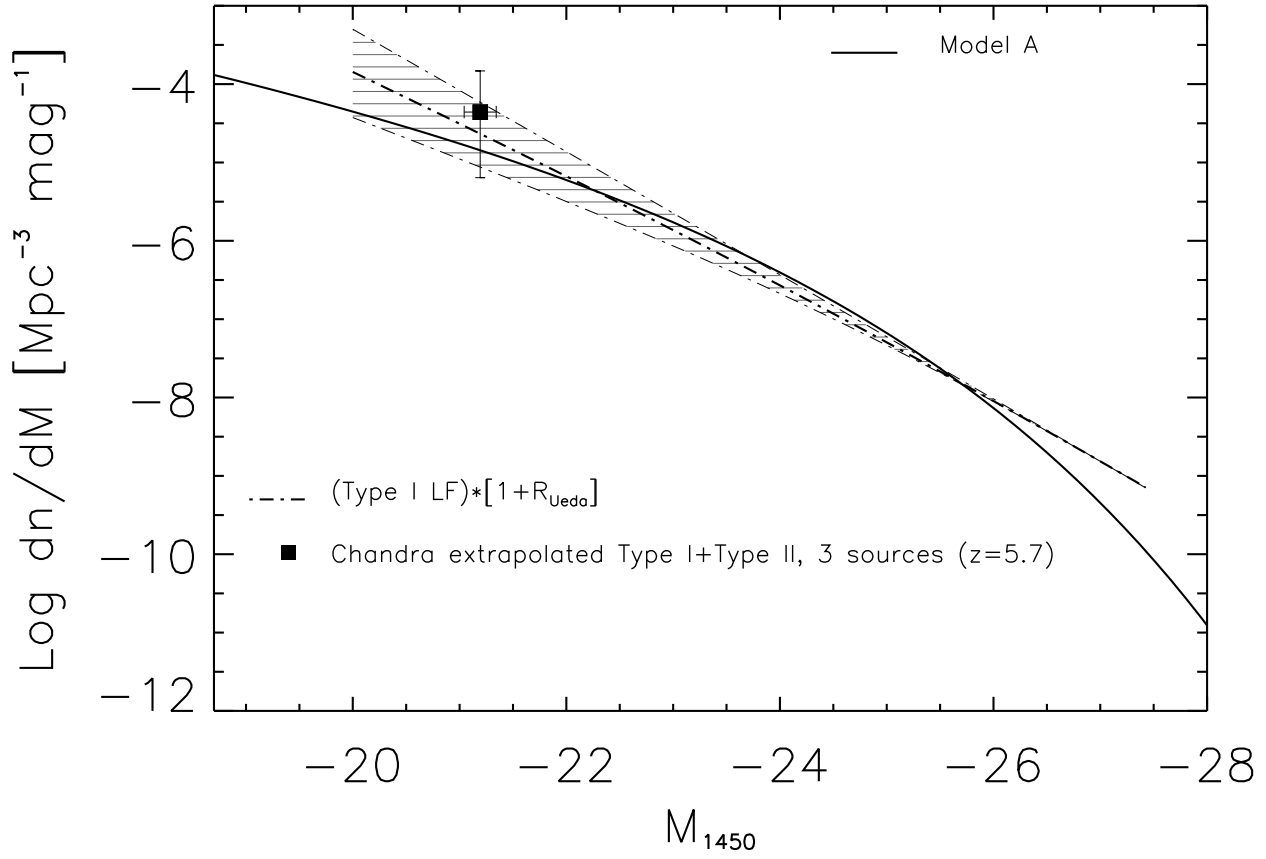


Fig. 3.— Estimated AGN luminosity function at $z \sim 6$ obtained by considering the average QSO luminosity function derived in section 3.1 (with its uncertainty region shown as a *striped* region) and multiplying it by $(1 + R_{\text{Ueda}})$, to account for all sources up to $\log N_H = 26 \text{ (cm}^{-2}\text{)}$. The *solid* line is the result of Model A (see text); all sources are assumed to radiate at the Eddington limit.

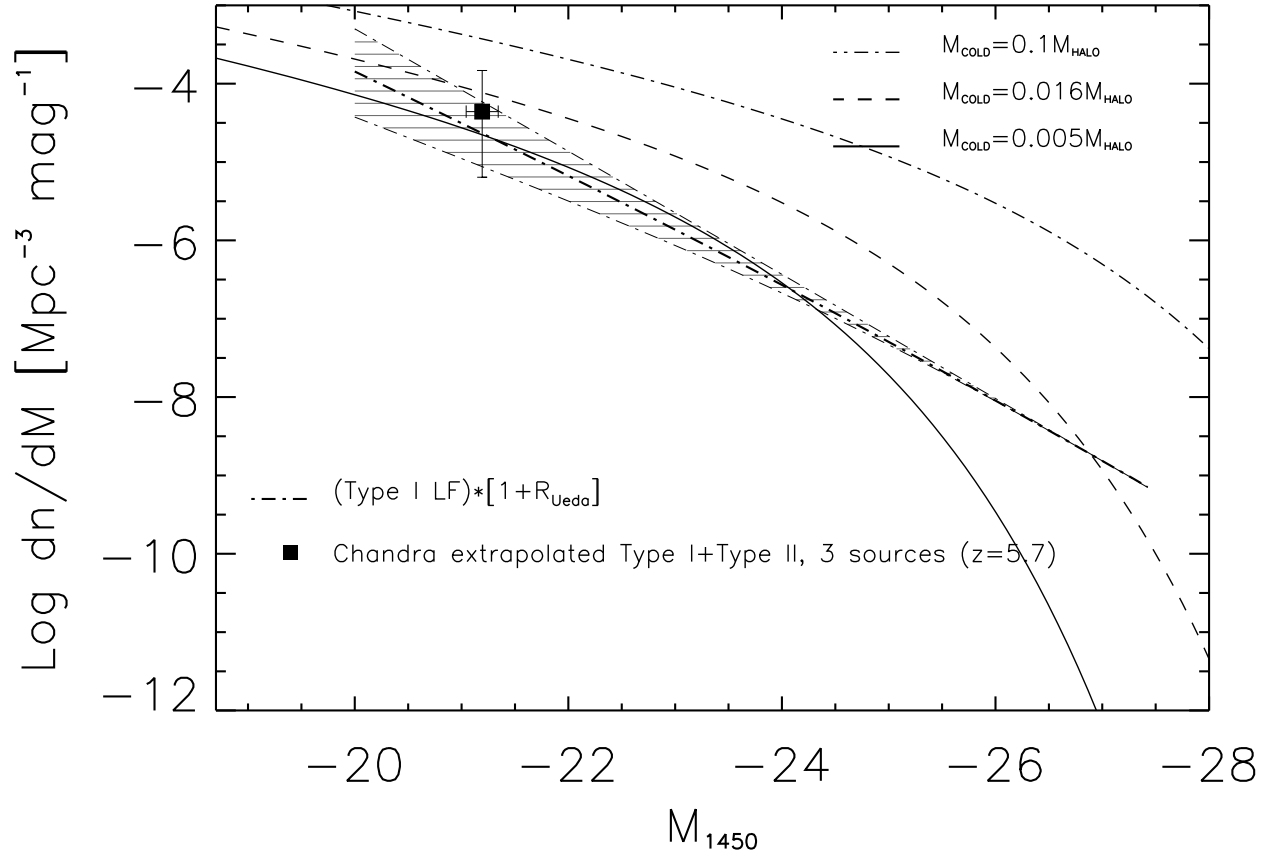


Fig. 4.— The *dot-dashed*, *dashed* and *solid* lines are the results of Model B (see text) for different fraction of cold gas with respect to the dark matter host mass as labeled; all sources are assumed to radiate at the Eddington limit. All the other curves are as in Figure 3.

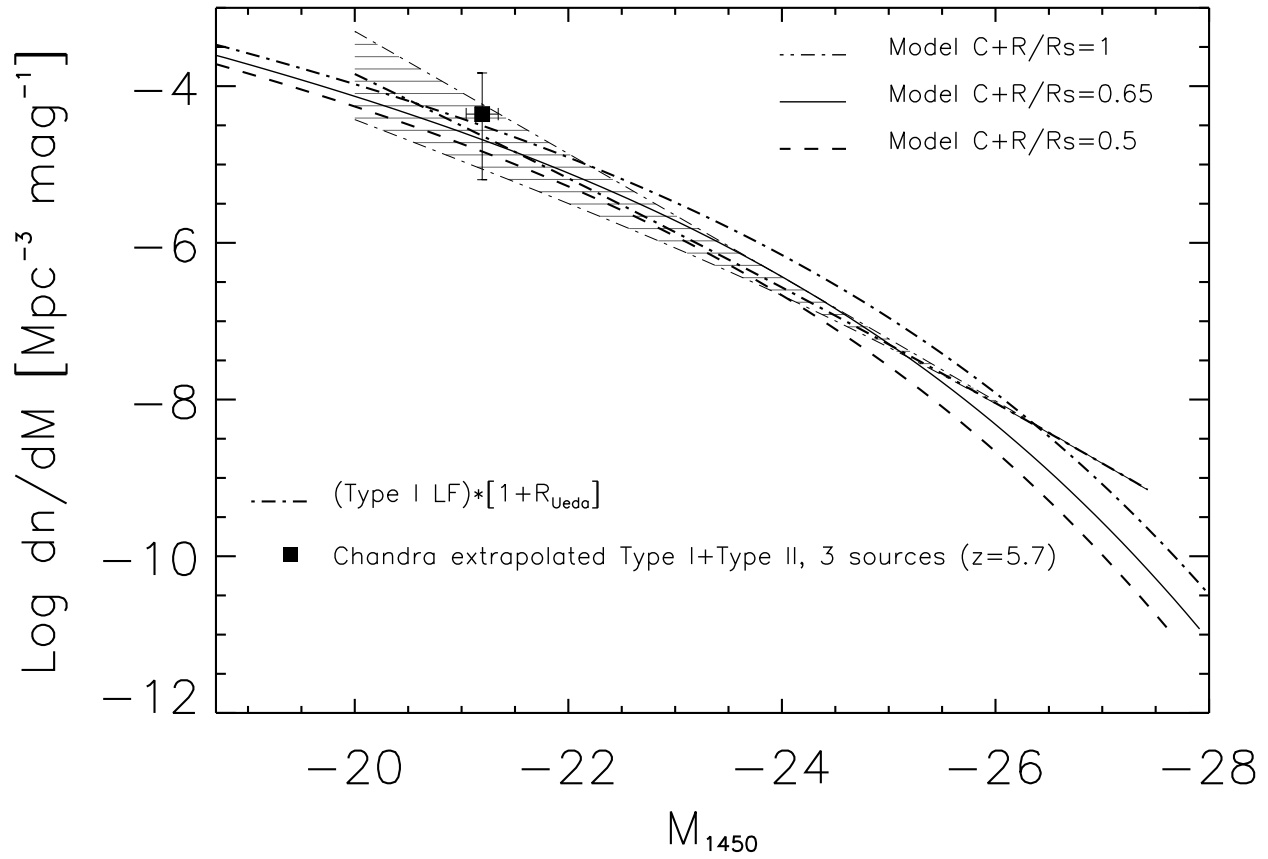


Fig. 5.— The *dot-dashed*, *dashed* and *solid* lines are the results of Model C (see text) for different R/R_s ratios as labeled, assuming that all sources are radiating at the Eddington limit. All the other curves are as in Figure 3.